Title

Computational modeling of drug transport and mixing in the chemofilter device: enhancing the removal of chemotherapeutics from circulation.

Journal

Biomechanics and Modeling in Mechanobiology, 19(5)

Authors

Maani, Nazanin
Diorio, Tyler
Hetts, Steven
et al.

Publication Date

2020-10-01

DOI

10.1007/s10237-020-01313-8

Peer reviewed

HHS Public Access

Author manuscript

Biomech Model Mechanobiol. Author manuscript; available in PMC 2024 January 27.

Published in final edited form as:

Biomech Model Mechanobiol. 2020 October ; 19(5): 1865–1877. doi:10.1007/s10237-020-01313-8.

Computational modeling of drug transport and mixing in the chemofilter device: enhancing the removal of chemotherapeutics from circulation

Nazanin Maani[1], **Tyler C. Diorio**[1], **Steven W. Hetts**[2], **Vitaliy L. Rayz**[1]

[1]Weldon School of Biomedical Engineering, Purdue University, West Lafayette, IN, USA

[2]Radiology and Biomedical Imaging, University of California San Francisco, San Francisco, CA, USA

Abstract

Intra-arterial chemotherapy (IAC) is the preferred treatment for non-resectable hepatocellular carcinoma. A large fraction of IAC drugs, e.g., Doxorubicin, pass into systemic circulation, causing cardiac toxicity and reducing effectiveness of the procedure. These excessive drugs can be captured by the Chemofilter—a 3D-printable, catheter-based device deployed in a vein downstream of the liver during IAC. In this study, alternative configurations of the Chemofilter device were compared by evaluating their hemodynamic and filtration performance through multiphysics computational fluid dynamics simulations. Two designs were evaluated, a honeycomb-like structure of parallel hexagonal channels (honeycomb Chemofilter) and a cubic lattice of struts (strutted Chemofilter). The computationally optimized Chemofilter design contains three honeycomb stages, each perforated and twisted, which improved Doxorubicin adsorption by 44.6% compared to a straight channel design. The multiphysics simulations predicted an overall 66.8% decrease in concentration with a 2.9 mm-Hg pressure drop across the optimized device compared to a 50% concentration decrease observed during *in-vivo* experiments conducted with the strutted Chemofilter. The Doxorubicin transport simulations demonstrated the effectiveness of the Chemofilter in removing excessive drugs from circulation while minimizing pressure drop and eliminating flow stagnation regions prone to thrombosis. These results demonstrate the value of the multiphysics modeling approach in device optimization and experimental burden reduction.

Keywords

Intra-arterial chemotherapy; Medical device; Multiphysics modeling; Computational fluid dynamics; Hemodynamics; Drug transport; Convection–diffusion; Adsorption; Mass transfer

1 Introduction

Liver cancer is the fourth leading cause of cancer-related mortality worldwide, accounting for 8.2% of total cancer deaths (Bray et al. 2018). Hepatocellular carcinoma (HCC), the

✉Vitaliy L. Rayz, vrayz@purdue.edu, Nazanin Maani, nmaani@purdue.edu.

Conflict of interest The authors declare that they have no conflict of interest.

primary liver cancer, accounts for approximately 85% of liver cancers in the USA (Bray et al. 2018). For cases that are not amenable to surgery, intra-arterial chemotherapy (IAC) is the preferred treatment for HCC (Roche 2003; Stuart 2003). In the context of hepatic IAC, a catheter is advanced through the femoral artery to the hepatic arteries that supply HCC tumors. Chemotherapeutic drugs, such as doxorubicin (Dox), are subsequently injected over the course of a 10 min period, depending on patient anatomy or specific tumor conditions. The IAC procedure allows targeted drug delivery to the tumor, in comparison to systemic intravenous chemotherapy. However, this technique is still associated with significant side effects, including irreversible heart failure, due to the 50–70% of IAC drugs that pass through the liver and affect other organs (Alexander et al. 2011, 2012; Aboian et al. 2016; Lewis et al. 2006). This greatly limits the ability to safely deliver high therapeutic doses of IAC drugs, such as Dox. Moreover, Dox has been shown to demonstrate a positive, linear relationship between dose and tumor suppression, suggesting that the ability to deliver higher doses may greatly affect treatment outcome (Curley et al. 1994; August et al. 1995; Ku et al. 1998, 2002; Porrata and Adjei 2001).

In order to decrease the side effects and increase the efficacy of the IAC procedure, a novel biomedical device, Chemofilter, has been suggested previously (Maani et al. 2018; Patel et al. 2014; Aboian et al. 2016; Oh et al. 2019). Chemofilter is a catheter-based endovascular device adsorbing chemotherapy drugs to a filtering surface to remove excess drugs from blood. The Chemofilter is temporarily deployed from a catheter in a vein distal to the organ undergoing IAC infusion and remains in place for the duration of the procedure. In the context of HCC, IAC would deliver Dox to the liver via the hepatic artery while the Chemofilter would capture the excess Dox as it exits through the hepatic veins or inferior vena cava (IVC) as shown in Fig. 1.

The chemotherapeutic drug, Dox, can be captured through three distinct mechanisms: ion-exchange (Oh et al. 2019), DNA binding (Aboian et al. 2016), or magnetic capture (Mabray et al. 2016; Wilson et al. 2004). The ion-exchange approach, which will be the mechanism considered in this study, utilizes an ion-exchange resin comprised of the block copolymer PtBS-PEP-PSS-PEP-PtBS, which coats the surface of a 3D-printable scaffold (Oh et al. 2019). Dox, which is a positively charged ion in the blood, reacts with the negatively charged sulfonate group of the resin on the Chemofilter to form a solid species that remains on the surface and thus gets eliminated from circulation.

The deployment of the Chemofilter can cause significant changes to local hemodynamics during treatment. A stagnant or recirculating flow forming near the Chemofilter may increase the risk of thrombosis (Lowe 2003; Ren et al. 2012). Moreover, since the Chemofilter is deployed in a low pressure part of the circulation, such as the IVC or hepatic veins, the pressure drop across the device should be controlled to minimize the risk of flow stagnation. Given that the pressure within the human IVC is approximately 10 mm Hg for healthy patients, pressure drop should not exceed 5–7 mm Hg to minimize the risk of flow stagnation according to clinical recommendation. The success of the Chemofilter as an intravascular catheter-based filtration device depends on its ability to remove Dox from blood in a safe and efficient manner.

In order to optimize the hemodynamic performance of the Chemofilter, alternative device designs and configurations were proposed and evaluated. As shown in Fig. 2, these different configurations fall under two general categories of porous (Fig. 2a) and non-porous membranes (Fig. 2b, c). The hemodynamic performance of the porous membrane device, which consists of architected material (a matrix of tessellated microscale unit-cells) forming an umbrella-shaped basket, has been previously investigated with computational fluid dynamics (CFD) simulations (Maani et al. 2018). In the current study, which is an extension of Maani et al. 2018, a multiphysics modeling approach of Dox transport through the Chemofilter and its binding to the ionic surface of the Chemofilter was developed. The in silico results were then compared to the drug filtration measured in vivo in porcine studies. Two alternative, non-porous Chemofilter configurations are optimized with CFD simulations to maximize drug binding while minimizing the pressure drop and flow obstruction. A comparative study was performed for evaluating different configurations utilizing an analogy between heat and mass transport mechanisms. The results obtained with this multi-physics modeling approach were compared with experimental results obtained in animal studies (Oh et al. 2019).

2 Methods

In order to evaluate and compare the performance of different Chemofilter designs, numerical simulations were conducted and results were compared with those obtained in porcine studies reported in Oh et al. (2019). The computational studies were conducted on two different configurations of the Chemofilter with a non-porous membrane: the *honeycomb* Chemofilter and the *strutted* Chemofilter. The strutted Chemofilter, used in experimental studies (Oh et al. 2019), consists of a uniform cubic lattice of struts as shown in Fig. 2b. The honeycomb Chemofilter, developed in computational studies (Fig. 2c), consists of parallel hexagonal channels which resemble the natural honeycomb. In the original, “plain” honeycomb design, hexagonal channels are aligned with the direction of blood flow. The upstream flow divides between the honeycomb’s cylindrical channels where Dox particles bind to the coated surfaces. In order to further enhance drug adsorption, the honeycomb channels can be (a) perforated to allow flow mixing between the channels, and (b) twisted to disrupt concentration boundary layer formation in the channels (Fig. 2c).

2.1 CFD simulations

For the CFD simulations of the Chemofilter, the geometry was generated in SolidWorks (SolidWorks Corp., Dassault Systèmes) software. To generate the flow domain in SolidWorks, the device was modeled in a straight tube, long enough to ensure fully developed flow upstream of the filter and prevent reversed flow at the outlet. For developing the honeycomb configuration in SolidWorks, hexagons were constructed with an apothem length of 0.50 mm and a corresponding edge length of 0.58 mm to construct the configuration with 0.90 mm diameter. In the perforated honeycomb models, channels were perforated in a spiral pattern such that each hole exposed an area of $0.4 \times 0.4\ mm^2$ to adjacent channels (Fig. 2c). In the plain and perforated honeycomb, 1/6th of the domain was considered with a symmetry boundary condition applied on the side walls to save

computational time and cost. However, full geometry modeling was required for the twisted configurations.

The CAD file was then imported to ANSYS ICEM (ANSYS, Inc.) for discretization and meshing. In order to ensure an adequate resolution for the flow within individual channels, the mesh density around the Chemofilter was increased to achieve a maximum size of 0.02–0.05 mm, resulting in between 2 and 4 million mesh elements total, depending on the geometry. Mesh independence of the numerical solution was confirmed for all configurations with negligible discrepancies in concentration and pressure drop (< 3%) when varying the number of elements around the Chemofilter by a factor of two. The discretized geometry was imported to ANSYS Fluent for numerical solution, and the results were processed using ANSYS CFD-Post software.

The coupled Navier–Stokes and advection-diffusion-reaction equations were solved with a finite-volume solver, ANSYS Fluent. A second-order scheme was used for pressure, and third-order MUSCL schemes were used for momentum, energy, and species transport spatial discretization. The flow was modeled as steady due to the negligible effect of the cardiac pulse in the hepatic vein, and the Reynolds number was low enough (Re = 300) for the flow to remain laminar. The inlet velocity was set to 0.1 m/s, and the outflow boundary condition was assigned to the outlet. To model Dox binding to the Chemofilter, the energy and species transport were activated in Fluent. The advectiondiffusion-reaction equation was solved, assuming a one-step reaction ($Dox^{+} + SO_3^{-} \rightarrow Dox - SO_3$) for the ionic binding. The reaction term was based on Arrhenius model, and the surface mass deposition source was activated in Fluent to account for the effect of surface mass transfer in the continuity equation.

The passive diffusion coefficient of Dox in blood (approximately 10^{-10} m^2/s) does not account for the effect of electrochemical forces and thus would result in underestimated drug adsorption for each device configuration. Dox particles, in addition to being transported due to advection and diffusion in blood, are attracted toward the ionic surface of the Chemofilter by electrochemical forces. The electrochemical forces are dominant in the Electric Double Layer adjacent to the ionic surface, where binding is considered spontaneous. The interplay of the electrochemical forces and hemodynamics result in a non-divergent free velocity field around the ionic surface, which adds a new term to the mass balance equation. The contribution of the electrochemical forces in the advection-diffusion-reaction equation can be represented by an effective diffusion coefficient which replaces the passive diffusion coefficient. The effective diffusion coefficient of Dox in blood adjacent to the Chemofilter surface derived according to the concentrated solution theory is approximately two orders of magnitude greater than the passive diffusion coefficient.

2.2 Heat transfer analogy

In this study, the analogy between the mass and heat transfer was utilized as a simple and tangible method for comparing the performance of different Honeycomb configurations. In order to use this analogy, the Schmidt number, i.e., the ratio of momentum and mass diffusivity, and the Prandtl number, i.e., the ratio of momentum and heat diffusivity, were matched. The Peclet number, expressing the ratio of diffusion to advection timescale was

also matched in both systems by setting the thermal diffusion coefficient equal to the mass transport effective diffusion coefficient. The flow conditions were identical for both models, thus maintaining the same velocity boundary layers. We note that in the above analogy, a constant diffusion coefficient of species was considered. In the simulations with heat transfer analogy, only the energy equation was activated. We note that using the heat transfer rather than the species transport module of the Fluent (ANSYS) modeling platform allowed us to enhance convergence and reduce simulation time. In addition, with this approach it was possible to avoid specifying mass transport parameters that were not yet available from the experimental studies of the device.

In the mass transport simulations, the Dox mass fraction was set to 0.005 at the inlet and the filter surface was modeled as a mass sink with unlimited binding sites, thus neglecting the saturation of the filter surface or adsorption of other proteins to the surface. In the analogous heat transfer simulations, the temperature of the inlet flow was set to 800 K and the thermal sink on the surface of the filter was modeled with a constant temperature of 300 K, resulting in the cooling of fluid as it passed through the filter. This model is analogous to the reduction in Dox concentration, with the drug adsorbing to the Chemofilter surface instead of heat being transferred. Since Dox does not adsorb to the vessel wall, the wall was set to be adiabatic in the thermal system. The effective diffusion coefficient, D_{eff}, accounting for the ionic migration, was calculated using the concentrated solution theory and found to be in the order of 10^{-8} m^2/s.

2.3 Parameter characterization and sensitivity analysis

In order to find the optimal honeycomb configuration, the sensitivity of the model to the various geometry and transport parameters was investigated. The following parameters were studied as presented in Table 1: (1) diameter of hexagonal channels, (2) twist angle of the channels, (3) length of the honeycomb channels, (4) spacing of multiple honeycomb sections in series, (5) inlet velocity, and (6) the diffusion coefficient. The flow boundary conditions and other vessel geometry parameters remained the same in all simulations. The diameter of hexagonal channels was varied from 0.45 to 0.90 mm to assess the benefit of decreasing the diameter on drug adsorption. The twist angle of the channels was varied from 0° for the plain honeycomb to 45° (corresponding to helix angle of 84°) and the honeycomb length was varied between 5.8 and 20 mm. In the staged configuration, the sensitivity of the results to the spacing between honeycomb sections was investigated by varying the spacing from 1.3 to 11.6 mm (staged configuration in Fig. 2). The inlet velocity was varied from 0.01 to 0.10 m/s to represent porcine and human venous hepatic blood flow velocity, respectively. The diffusion coefficient of Dox in blood was varied from 10^{-7} to 10^{-10} m^2/s to compare the effect of effective diffusion by the ion-exchange resin to passive diffusion.

To evaluate the sensitivity of the results to design parameters and intrinsic properties (the diameter of hexagonal channel, the inlet velocity, and diffusion coefficient), the Cotter's method for sensitivity analysis was utilized (Cotter 1979). Cotter's method allows ranking the input design parameters based on their influence on the overall binding performance. The channel diameter range was varied by a factor of two, and the velocity range was varied one order of magnitude. In the sensitivity analysis, we considered the variations of

the passive diffusion coefficient, which was varied by one order of magnitude (diffusion coefficient of 10^{-9} m^2/s used as the upper bound) in order to maintain a comparable effect of the different variables on the results.

2.4 Comparison to in-vivo experiments carried out for strutted Chemofilter

Preliminary animal studies were conducted at the UCSF using the strutted Chemofilter configuration (Oh et al. 2019), and therefore, the flow and transport through this configuration were also modeled in order to compare its performance with that of the proposed honeycomb configuration. In the animal studies, two strutted Chemofilter devices with 5 mm diameter were placed in parallel in the porcine IVC, as described in Oh et al. (2019). Dox was continuously injected during the first 10 min of the study, and the concentration downstream and upstream of the device was measured during this time period. In order to compare the computational results with available in vivo data, two 30 mm long strutted Chemofilters deployed in parallel were modeled. Since the actual diameter and velocity in the vein were not measured in the experimental study, the model assumed an oval cross section, with a gap between the filters and the wall of the vein. The hydraulic diameter of the stretched elliptical vein was matched with the 10 mm vessel diameter in the other simulations. The geometry of a strutted configuration with 10 mm diameter, termed the single strutted Chemofilter, was also modeled as an alternative configuration to be deployed in the IVC during future animal studies. For the single strutted Chemofilter, a quarter of the domain was considered and symmetry boundary conditions were applied to the side walls. For the parallel strutted Chemofilter, half of the elliptical domain, cut along the long axis of the ellipse, was modeled using symmetry boundary condition.

3 Results

3.1 Honeycomb configurations

The performance of alternative Chemofilter configurations was evaluated based on their hemodynamics and transport effectiveness using the heat and mass transport analogy. In Fig. 3, four configurations of the honeycomb Chemofilter are compared based on their respective filter surface area and temperature drop across the device. The length and diameter of all configurations were kept at 5.8 mm and 10 mm, respectively. The plain honeycomb with straight hexagonal channels delivered a temperature drop of 112 K (equivalent to 22.4% Dox mass reduction) with a corresponding pressure drop of 99 Pa (Fig. 3a). By perforating the channel walls (Fig. 3b), the ΔT increased by 5.36% to 119 K (equivalent to 23.8% Dox mass reduction) and ΔP decreased to 98 Pa. The addition of a 45° twist angle of the honeycomb channels resulted in a 13.4% increase in ΔT to 127 K (equivalent to 25.4% Dox mass reduction) with a corresponding pressure drop of 141 Pa (Fig. 3c). Combining the perforations with a 45° twist angle produced the largest ΔT of 151 K (equivalent to 30.2% Dox mass reduction) and a resulting ΔP of 116 Pa. Comparing the twisted-perforated honeycomb to the plain honeycomb, there was a 34.8% improvement in cooling, implying a similar increase in Dox capture.

In order to verify that the heat transfer analogy adequately represented the filtration of Dox, the results for both transport models were compared as shown in Fig. 4, showing

the temperature drop (a) and Dox mass reduction (b) across the device simulated for identical honeycombs at identical flow conditions. The temperature and molar fraction were normalized relative to the maximum change of the variable, i.e., $\Delta T^* = \frac{\Delta T}{\Delta T_{\text{Max}}}$ and $\Delta X^* = \frac{\Delta X}{\Delta X_{\text{Max}}}$, where $\Delta T_{\text{Max}} = 500$ and $\Delta X_{\text{Max}} = 0.005$. In the case shown in Fig. 4, the normalized changes in temperature and Dox mass fraction were both predicted to be 0.42 for the heat and species transport models, respectively. In addition, the matching patterns in the heat maps prove the accuracy of the provided analogy.

3.1.1 Parameter characterization and sensitivity analysis—In order to optimize the geometry of the twisted-perforated honeycomb, the sensitivity of temperature and pressure changes to the parameters stated in Table 1 was studied. Figure 5a shows that the temperature drop for a plain, 16 mm long honeycomb can be increased from 215 to 387 K (from 43% to 77.4% Dox capture) by decreasing the channel size from 0.90 to 0.45 mm, due to doubling the overall Chemofilter surface area and reducing by half the Peclet number. However, the pressure drop for this configuration with tighter channels increased 3.75 times. The effect of the twist angle on the perforated honeycomb with 5.8 mm length is demonstrated in Fig. 5b. The temperature drop increased from 119 to 151 K (from 23.8 to 30.2% Dox capture) by increasing the twist angle from 0° to 45°, and however, the pressure drop also increased from 98 to 116 Pa. The effect of the filter length on cooling performance was evaluated in terms of ΔT per unit length. For example, Fig. 5c shows that the cooling effectiveness of a 45° twisted-perforated honeycomb decreased from 26.0 to 17.6 K/mm as the length of the honeycomb increased from 5.8 to 20 mm, due to the formation of boundary layers within the channels. However, the pressure drop per length was uniform as expected. A Cotter's sensitivity analysis was performed on channel diameter, flow condition, and diffusion coefficient (marked by [a] in Table 1). Figure 5d demonstrates that the diffusion coefficient is the dominant factor which defines the binding performance. The overall range of the studied parameters is summarized in Table 1.

3.2 Final design: staged honeycomb Chemofilter

The decrease in the cooling rate of the fluid (or equivalent drug binding) along the length of the Chemofilter can be addressed by replacing a long continuous honeycomb by a series of shorter honeycomb sections. A proper spacing distance between sections of the staged honeycomb configuration disrupts the flow and concentration boundary layers that are formed in the channels, and allows re-mixing of the flow prior to entering the channels of the next honeycomb section. Although many simulations were conducted to optimize the design, six representative models with the channel twist angles of 30° and 45° were chosen for the simulations comparing the continuous and staged configurations as shown in Table 2. By comparing temperature drop per unit length in alternative configurations (i.e., model #1 vs. #2 and #5 vs. #6), it can be concluded that staged device configurations provide greater cooling performance per unit length than the continuous configurations. The effect of spacing distance can be observed in comparing the models #1 and #2. Though both have the nominal lengths of 20 mm, the continuous configuration has a smaller $\Delta T/L$ than the staged model, implying the same trend for the drug mass fraction reduction.

The effectiveness of individual honeycomb stages for models # 2, 3, 4, and 6 (Table 2) are demonstrated in Fig. 6. Comparing the three stages of model #2 and #6 shows that by providing larger spacing, the performance of the second and third stages increased. In addition, the overall cooling per unit length increased from 17.5 K/mm for model #2 to 19.2 K/mm for model #6 due to increased twist angle. Another strategy for increasing the effectiveness of the staging was to change the flow direction by twisting the channels of the intermediate stage in the direction opposite to the twist of the adjacent stages. The increase in mixing through the introduction of centripetal forces is shown by models #3 and #4 in both Table 2 and Fig. 6. Table 2 shows only 2% improvement in the cooling due to reversing the twist direction of the second stage. Therefore, the overall performance of each section of models #3 and #4 are approximately equal, with HC1 and HC2 contributing about 60% and 40% of total cooling, respectively (Fig. 6).

The results of the above simulations were used to determine the optimal Chemofilter design to be used in the next phase of animal studies. Figure 2c demonstrates the progression and schematics of the optimized honeycomb Chemofilter, with a length, channel diameter, twist angle, and spacing of 5.8 mm, 0.90 mm, 45°, and 5.8 mm, respectively.

3.3 Comparison to in-vivo experiments carried out for strutted Chemofilters

The strutted configurations, which were tested in porcine animal studies, are 5 mm in diameter and 30 mm in length (Oh et al. 2019). Multiple devices (9–12) were deployed into the pig's IVC and hepatic veins during the in vivo studies. Due to the larger diameter of the IVC compared to the hepatic veins, the devices were placed next to each other in parallel to fill the lumen. The computational models of parallel and single strutted Chemofilter devices are compared to the continuous honeycombs of identical length in Table 3. These simulations of the strutted devices deployed in parallel, predicted a ΔT of 117 K (equivalent to 23.4% in Dox mass reduction) and ΔP of 146 Pa (Figs. 2b, 8a, and Table 3). The single strutted configuration provided an overall 40.4% reduction in temperature, 202 K (or 40.4% Dox filtration), with a corresponding ΔP of 288 Pa, while the plain honeycomb provided a 43.0% reduction in ΔT, 215 K (or 43.0% Dox filtration), with a corresponding ΔP of 281 Pa. Despite the 2.35 times larger surface area, the plain honeycomb configuration resulted in almost the same ΔP. However, the cooling increased to 62.2%, with a ΔT of 311 K (equivalent to 62.2% Dox filtration) in the twisted-perforated honeycomb. Moreover, the optimized staged configuration provided a 66.8% decrease in temperature with a corresponding ΔP of 391 Pa (2.9 mm Hg).

The temperature drop along the length of the Chemofilter for alternative designs is shown in Fig. 7. The entrance region of each device demonstrates the greatest rate of temperature drop. The strutted design (model #8) demonstrates the lowest slope due to the unidirectional flow it promotes, while the continuous and staged honeycombs (models #5, 6, 10) demonstrate greater slopes. The staged honeycomb configuration (model #6) performed better for the longer device, as shown by the continuous decrease in temperature. Numerical results predict a threefold improvement in cooling by the staged honeycomb compared to the parallel strutted Chemofilter. These results are also visualized as temperature contours in Fig. 8. A corresponding improvement in the drug capture can be expected.

4 Discussion

4.1 Honeycomb configurations

The mass and heat transfer analogy was used to evaluate and optimize the Chemofilter design. In this analogy, the temperature drop of a hot fluid passing through the cold device was used to represent the change in the drug concentration due to adsorption. As stated above, simulating heat transfer rather than species transport allowed us to reduce computational time and the number of empirical parameters prescribed to the solver. The channels closer to the vessel wall experienced larger temperature drop (equivalent to drug adsorption) because of the slower velocity and larger flow residence time. The near-wall channels, which are not full hexagons, have the lowest velocity and therefore resulted in the greatest temperature drop as demonstrated in Figs. 3 and 4.

Since the passive diffusion of Dox in blood is low, the advection is dominant everywhere in the flow except in the near-wall region, as indicated by the average Peclet number in the order of 10^5. Therefore, the slow diffusion of Dox in blood can be compensated for by increasing the length of the channels to provide larger residence time, and thus allow more Dox particles to diffuse toward the surface. At the same time, the preliminary in vitro and in vivo studies showed that drug binds to the entrance region of the Chemofilter more effectively, which is supported by computational studies. Flow mixing in the entrance of the channels facilitates adsorption, as the concentration gradient is higher at the entrance. The boundary layers forming in the channels act like a transport insulator, thus decreasing the rate of drug adsorption unless the geometry or flow conditions change. One way of enhancing the mixing is to perforate the honeycomb channels to allow the flow from one channel to mix with the adjacent ones, as shown in Fig. 3b.

The mixing can be further enhanced by twisting the honeycomb channels in order to induce secondary flow. The effectiveness of twisting can be estimated by the dimensionless Dean number. In the twisted honeycomb, the channels closer to the center of the vessel have the Dean number of 60, which is the threshold for the appearance of Dean's vortices. The Dean number decreases in the channels away from the center due to the lower Reynolds number, even though the radius of curvature is increased. The low inertia of flow in the vein limits the effect of centripetal forces on the development of the secondary flow. However, in the near-wall channels lower velocity results in a smaller Peclet number, which compensates for the absence of Dean vortices due to larger residence time.

The results shown in Fig. 3b–c demonstrate that perforation and twisting of the channels provides increased temperature drop across the device, with the design combining both features delivering the best performance for the honeycomb configuration. In the twisted-perforated model, the flow is not isolated in the individual channels and the formation of fully developed flow is disrupted due to the secondary flow. It should be noted that the total surface area of the twisted-perforated honeycomb was reduced relative to the plain configuration, while the cooling was further increased. Figure 5b shows that by increasing the twist angle, the binding increases while the pressure drop remains below the estimated threshold for flow stagnation (5–7 mm Hg) in the hepatic vein and therefore the 45° twist angle was suggested for the honeycomb prototype.

4.2 Parameter characterization and sensitivity analysis

Decreasing the diameter of channels resulted in larger adsorption (Fig. 5a), since the total area in contact with the flow increased. Consequently, the number of binding sites increased, while the diffusion length scale decreased. The ideal Chemofilter configuration provides maximal drug capture and low pressure drop, with minimal reduction in adsorption rate along the Chemofilter. However, the smaller channels resulted in larger pressure drop due to increased resistance to the flow. Based on the mass and heat transfer correlations derived by Sieder–Tate for laminar flow (Welty 1984), the pressure drop and mass/heat transfer in a cylindrical channel change proportional to D^{-2} and $D^{-4/3}$, respectively. Therefore, a cross-point between the two parameters does not exist, as both trend asymptotically in the same direction. As a result, the optimum size of the channels can only be decided by setting a safe threshold for pressure drop to avoid stagnation of the venous flow.

The temperature/mass fraction and pressure drop per unit length provide a measure for characterizing different device configurations and ranking their effectiveness. The pressure drop is only a function of length, for a given channel size, and therefore is constant along the filter's unit length, but the temperature gradient decreases along the channel due to formation of the boundary layers. To avoid the fully developed boundary layer, the channel's length should be shorter than the entrance length. Figure 5c also shows that shorter honeycombs have larger temperature change per unit length, corresponding to increased rate of filtration per length.

Among the three honeycomb configuration parameters that were studied (channel diameter, twist angle, and Chemofilter length), the dominant parameter was the channel diameter, which caused a twofold increase in temperature drop when decreased by half in size. The passive diffusion coefficient in this study was increased in order to match an estimated effective diffusion coefficient accounting for the effect of electrochemical forces which may dominate the drug binding. The variation in the average vein velocity is due to the difference between the human and porcine circulation. Utilizing the effective diffusion coefficient in the simulations of porcine blood flow with an average velocity of 0.01 m/s through the Chemofilter ensured an agreement between the computational and experimental results. Guided by the above results, the diffusion coefficient used in this study was increased to 10^{-7} m^2/s, to match the resulting Peclet number (in the range of 225–450) for the human venous flow. The results suggest that the dominant parameter determining the binding effectiveness is the diffusion coefficient.

4.3 Final design: staged honeycomb Chemofilter

A staged configuration of the device was suggested in order to utilize the high effectiveness of short honeycomb stages without compromising the required surface area of the device. The ideal staging of the devices would result in equal effectiveness of all stages, which means that the flow would be properly mixed before entering each stage. The effect of spacing between the short honeycomb sections was investigated in simulations where the spacing of 1.3, 5.8, and 11.6 mm was used. For example, comparing the continuous model #1 and staged model #2 with 1.3 mm spacing distance, both with identical nominal lengths of 20 mm, the continuous configuration has an overall larger ΔT than the staged model.

This is due to insufficient distance for mixing between the stages. Therefore, a short spacing distance only results in reduction in the surface area without utilization of the benefits of the staged configuration. The results show that spacing equal to or larger than the length of the stage provides sufficient flow mixing before it enters the next stage. Another important benefit of staging the honeycombs is the improved flexibility in device deployment. The number of required Chemofilter stages can be decided by clinicians based on the location of the catheter and patient's vascular anatomy. The benefit of using stages with alternating direction of the twist angle of the channels was also studied. Due to the low inertia of venous flow, this feature was not found to have a significant effect on the resulting temperature changes ($De < 60$).

4.4 Comparison to in-vivo experiments carried out for strutted Chemofilter

The strutted device configurations were developed and used in animal studies to examine the electrochemical binding mechanism which was developed for capturing Dox from the blood stream. In the hepatic veins with diameter of 5 mm, the placement of filters with corresponding size resulted in a close fit in the vein without a gap near the wall. However, the same filter deployed in the IVC moved next to the wall following the guide wire, and the main flow bypassed it. Therefore, two strutted devices were deployed in parallel in the IVC to compensate for this effect. With the placement of two parallel Chemofilters in the hepatic vein, the cross section of the vein was assumed to deform to an oval, resulting in the formation of regions of low resistance in the gaps between the vessel wall and the two filters. The gap led to high velocity regions forming between the parallel filters (Fig. 8a), which allowed 63% of blood flow to pass unfiltered, thus resulting in inefficient filtration. Since the gap reduced the resistance to flow, the overall pressure drop across the device was low. However, this decreased resistance also caused a decrease in filtration efficiency. The analysis of the effect of the near-wall gap on device filtration was reported previously in Maani et al. (Maani et al. 2018). The performance of the strutted Chemofilters illustrated in Fig. 8a, b is also quantified in Table 3. The models of the parallel and single strutted configurations demonstrate that by correctly fitting the device to the intended site of deployment, the overall temperature change downstream of the device improved by 72.6% compared to the parallel strutted configuration, as shown in Table 3 and Fig. 8. The overall performance of the single strutted filter was comparable to that of the plain, un-optimized honeycomb.

Oh et al. (2019) reported that the strutted Chemofilter delivered a decrease in Dox concentration of $64 \pm 6\%$ following the 10-min injection period. In their study it was assumed that 100% of excess Dox was present in the plasma samples; however, it is likely that only about 85% of Dox is present in the plasma (ASoHSP 2009). By accounting for this discrepancy, the experimental Dox concentration change reported by Oh et al. becomes $54 \pm 5\%$. The computational model of the same device configuration (parallel strutted Chemofilter with inlet velocity of 0.01 m/s) estimated that 50% of Dox would be eliminated from the blood stream, which approximately matches the adjusted results reported by Oh et al. (2019). Despite the observed success of the strutted Chemofilter configuration in achieving significant reduction of the Dox concentrations (Oh et al. 2019), computational

models suggest that the filtration performance can be further improved by using the staged honeycomb Chemofilter.

4.5 Comparison of the non-porous honeycomb and porous Chemofilter basket configurations

The Chemofilter configuration incorporating a porous membrane formed by a lattice of micro-cells (Maani et al. 2018) was designed to be 3D printed and attached to a to a nitinol frame shaped like a basket. This design was inspired by the RX-Accunet device which is widely used in clinical practice. The honeycomb Chemofilter considered in the current study was also designed to be 3D printed from an elastic polymer which can be crimped into a catheter for deployment. The flow channels of the honeycomb prototype are about an order of magnitude larger than those of the non-porous membrane. This leads to a difference in the corresponding surface area, flow resistance, and residence time. The manufacturing of the honeycomb Chemofilter is more feasible due to its larger scale. The CFD results showed the pressure drop of 320 Pa for the porous Chemofilter basket, where the surface area and the thickness of the membrane were 940 mm^2 and 0.3 mm, respectively. This pressure drop was comparable to that of 391 Pa computed for the honeycomb, while the surface area and length of the honeycomb were 4800 mm^2 and 17.4 mm. In this study it was assumed that the Chemofilter surface had unlimited binding sites and the surface saturation was also neglected. It is likely that in reality, the larger surface area of the honeycomb Chemofilter would provide a larger number of the binding sites, thus making the honeycomb configuration a better option than the porous membrane basket or the strutted configuration.

5 Limitations and future work

In reality, the binding of Dox to the ionic resin is driven by electrochemical forces attracting the particles toward the surface. The electrochemical binding is considered by applying the concentrated solution theory approximation, to be addressed in more detail in a report that will be published separately.

Moreover, a direct comparison between the available animal studies and computational results is challenging due to the limitations of the animal study protocol. In particular, during in vivo studies the exact cross-sectional area, Chemofilter position in the vein, and blood velocity in the vein were not measured; therefore, the values used in the CFD simulations were assumed or taken from the literature. To address this problem, Doppler ultrasound measurements will be performed during the next experiments to obtain the accurate cross-sectional area and vein velocity, thus enabling a fair comparison of the results. It should be noted that the strutted Chemofilter used for in vivo studies contained active sites on the outer surface of the device, where it may contact the vessel wall, whereas in the optimization simulations this area is treated as a non-binding wall and the performance was underestimated.

Also, in this study the blood velocity in the vein was based on values observed in the human IVC, while the velocity in the porcine IVC is about one order of magnitude lower than that of human. Nevertheless, since the flow and transport conditions remained the same in all CFD studies of the alternative device configurations, the results and conclusions are valid

for a comparison. Based on the results presented in this study, the future in vitro and in vivo studies will be performed with the optimized honeycomb device and the drug concentration will be compared to the previous set of studies with the strutted Chemofilter.

6 Conclusion

In this study, the configuration of the Chemofilter device intended for filtering excessive chemotherapy drugs from blood was optimized with multiphysics CFD modeling. The hemodynamic performance and drug elimination efficiency of a honeycomb-shaped device was compared with that of a strutted Chemofilter, previously tested in animal studies. Utilizing the analogy between the heat and mass transport, a numerical model for evaluating drug transport and chemical binding was developed. The honeycomb-shaped configuration containing multiple parallel channels provided increased surface area for drug binding. The mixing and binding of the drug can also be enhanced by using twisted and perforated channels, which result in 44.6% improvement compared to the straight channel design for a honeycomb with the same length. A staging of the honeycomb devices in series is suggested to further increase the overall efficiency of the device, which also provides flexibility for deployment of the device during catheterization. A shorter length of each honeycomb stage facilitated mixing; moreover, using multiple stages provided the required residence time for the adsorption of drug particles. The comparison of the honeycomb and strutted Chemofilters demonstrated the superior performance of the optimized honeycomb configuration, evidenced by an estimated 66.2% improvement in drug capture. Computational simulations allowed the performance of different Chemofilter device configurations to be evaluated, enabling device optimization with minimal need for in vivo experiments.

Acknowledgements

We like to acknowledge Dr. Nitash Balsara and his group for providing the details of the animal study and Dr. Mark Wilson for his insights into the clinical concerns for the Chemofilter design during animal studies. We also acknowledge Teri Moore for coordinating the study and data exchange.

Funding

The work presented was funded by NIH grants 1R01CA194533 (Steven Hetts, PI; UCSF), 1R41CA183327 (Anand Patel, PI; ChemoFilter, Inc.). A patent underlying the Chemofilter technology was licensed to Chemofilter, Inc, by the University of California; that license was subsequently incorporated in the acquisition of Chemofilter, Inc by Penumbra, Inc (Alameda, California). Chemofilter is a trademark of Penumbra, Inc.

References

Aboian MS, Yu JF, Gautam A, Sze CH, Yang JK, Chan J, Lillaney PV, Jordan CD, Oh HJ, Wilson DM, Patel AS, Wilson MW, Hetts SW (2016) In vitro clearance of doxorubicin with a DNA-based filtration device designed for intravascular use with intra-arterial chemotherapy. Biomed Microdevices 18(6):98. 10.1007/s10544-016-0124-5 [PubMed: 27778226]

Alexander CM, Maye MM, Dabrowiak JC (2011) DNA-capped nanoparticles designed for doxorubicin drug delivery. Chem Commun 47(12):3418–3420

Alexander CM, Dabrowiak JC, Maye MM (2012) Investigation of the drug binding properties and cytotoxicity of DNA-capped nanoparticles designed as delivery vehicles for the anticancer agents doxorubicin and actinomycin D. Bioconjugate Chem 23(10):2061–2070

American Society of Health System Pharmacists (ASoHSP) (2009) AHFS drug information 2009. Bethesda, MD

August DA, Verma N, Vaerten MA, Shah R, Andrews JC, Brenner DE (1995) Pharmacokinetic evaluation of percutaneous hepatic venous isolation for administration of regional chemotherapy. Surg Oncol 4(4):205–216. 10.1016/S0960-7404(10)80037-4 [PubMed: 8528483]

Bray F, Ferlay J, Soerjomataram I, Siegel RL, Torre LA, Jemal A (2018) Global cancer statistics 2018: GLOBOCAN estimates of incidence and mortality worldwide for 36 cancers in 185 countries. Cancer J Clin 68(6):394–424

Cotter SC (1979) A screening design for factorial experiments with interactions. Biometrika 66(2):317–320. 10.2307/2335664

Curley SA, Newman RA, Dougherty TB, Fuhrman GM, Stone DL, Mikolajek JA, Guercio S, Guercio A, Carrasco CH, Kuo MT et al. (1994) Complete hepatic venous isolation and extracorporeal chemofiltration as treatment for human hepatocellular carcinoma: a phase I study. Ann Surg Oncol 1(5):389–399 [PubMed: 7850540]

Ku Y, Iwasaki T, Fukumoto T, Tominaga M, Muramatsu S, Kusunoki N, Sugimoto T, Suzuki Y, Kuroda Y, Saitoh Y, Sako M, Matsumoto S, Hirota S, Obara H (1998) Induction of long-term remission in advanced hepatocellular carcinoma with percutaneous isolated liver chemoperfusion. Ann Surg 227(4):519–526 [PubMed: 9563540]

Ku Y, Tominaga M, Iwasaki T, Fukumoto T, Kuroda Y (2002) Isolated hepatic perfusion chemotherapy for unresectable malignant hepatic tumors. Int J Clin Oncol 7(2):82–90. 10.1007/s101470200011

Lewis AL, Taylor RR, Hall B, Gonzalez MV, Willis SL, Stratford PW (2006) Pharmacokinetic and safety study of doxorubicineluting beads in a porcine model of hepatic arterial embolization. J Vasc Interv Radiol 17(8):1335–1343. 10.1097/01.rvi.0000228416.21560.7f [PubMed: 16923981]

Lowe GDO (2003) Virchow's triad revisited: abnormal flow. Pathophysiol Haemost Thromb 33(5–6):455–457 [PubMed: 15692260]

Maani N, Hetts SW, Rayz VL (2018) A two-scale approach for CFD modeling of endovascular Chemofilter device. Biomech Model Mechanobiol 17(6):1811–1820. 10.1007/s10237-018-1058-z [PubMed: 30066295]

Mabray MC, LiHaney P, Sze CH, Losey AD, Yang J, Kondapavulur S, Liu D, Saeed M, Patel A, Cooke D, Jun YW, El-Sayed I, Wilson M, Hetts SW (2016) In vitro capture of small ferrous particles with a magnetic filtration device designed for intravascular use with intraarterial chemotherapy: proof-of-concept study. J Vasc Interv Radiol 27(3):426–432. 10.1016/j.jvir.2015.09.014 [PubMed: 26706187]

Oh HJ, Aboian MS, Yi MYJ, Maslyn JA, Loo WS, Jiang X, Parkinson DY, Wilson MW, Moore T, Yee CR, Robbins GR, Barth FM, DeSimone JM, Hetts SW, Balsara NP (2019) 3D printed absorber for capturing chemotherapy drugs before they spread through the body. ACS Cent Sci 5(3):419–427. 10.1021/acscentsci.8b00700 [PubMed: 30937369]

Patel A, Saeed M, Yee E, Yang J, Lam G, Losey AD, Lillaney P, Thorne B, Chin A, Malik S, Wilson M, Chen XC, Balsara N, Hetts S (2014) Development and validation of endovascular chemotherapy filter device for removing high-dose doxorubicin: preclinical study. J Med Devices 8(4):0410081–410088. 10.1115/1.4027444

Porrata LF, Adjei AA (2001) The pharmacologic basis of high dose chemotherapy with haematopoietic stem cell support for solid tumours. Br J Cancer 85(4):484–489. 10.1054/bjoc.2001.1970 [PubMed: 11506483]

Ren Z, Wang S, Singer M (2012) Modeling hemodynamics in an unoccluded and partially occluded inferior vena cava under rest and exercise conditions. Med Biol Eng Comput 50(3):277–287. 10.1007/s11517-012-0867-y [PubMed: 22354383]

Roche A (2003) Trans-catheter arterial chemoembolization as first-line treatment for hepatic metastases from endocrine tumors. Eur Radiol 13(1):136 [PubMed: 12541121]

Stuart K (2003) Chemoembolization in the management of liver tumors. Oncologist 8(5):425–437. 10.1634/theoncologist.8-5-425 [PubMed: 14530495]

Welty JR (1984) Fundamentals of momentum, heat, and mass transfer, 3rd edn. Wiley, New York

Wilson MW, Kerlan RK Jr, Fidelman NA, Venook AP, LaBerge JM, Koda J, Gordon RL (2004) Hepatocellular carcinoma: regional therapy with a magnetic targeted carrier bound to doxorubicin

in a dual MR imaging/conventional angiography suite–initial experience with four patients. Radiology 230(1):287–293. 10.1148/radiol.2301021493 [PubMed: 14695402]

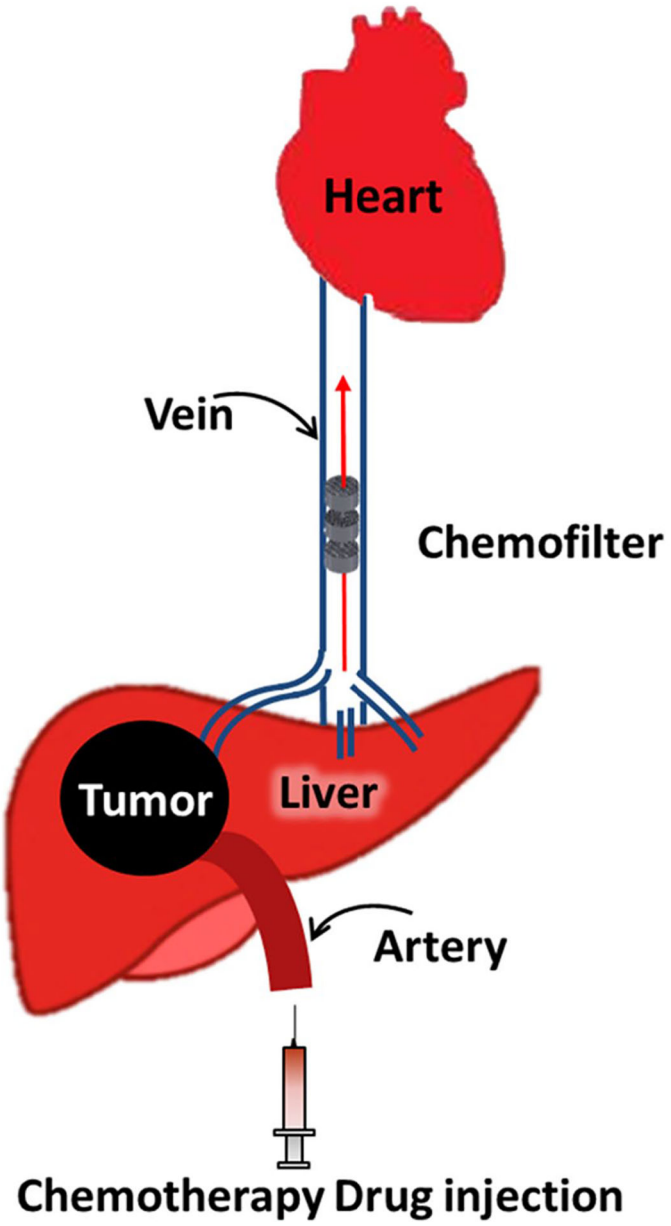

Fig. 1.
A schematic of the hepatic IAC procedure and Chemofilter deployment in the IVC

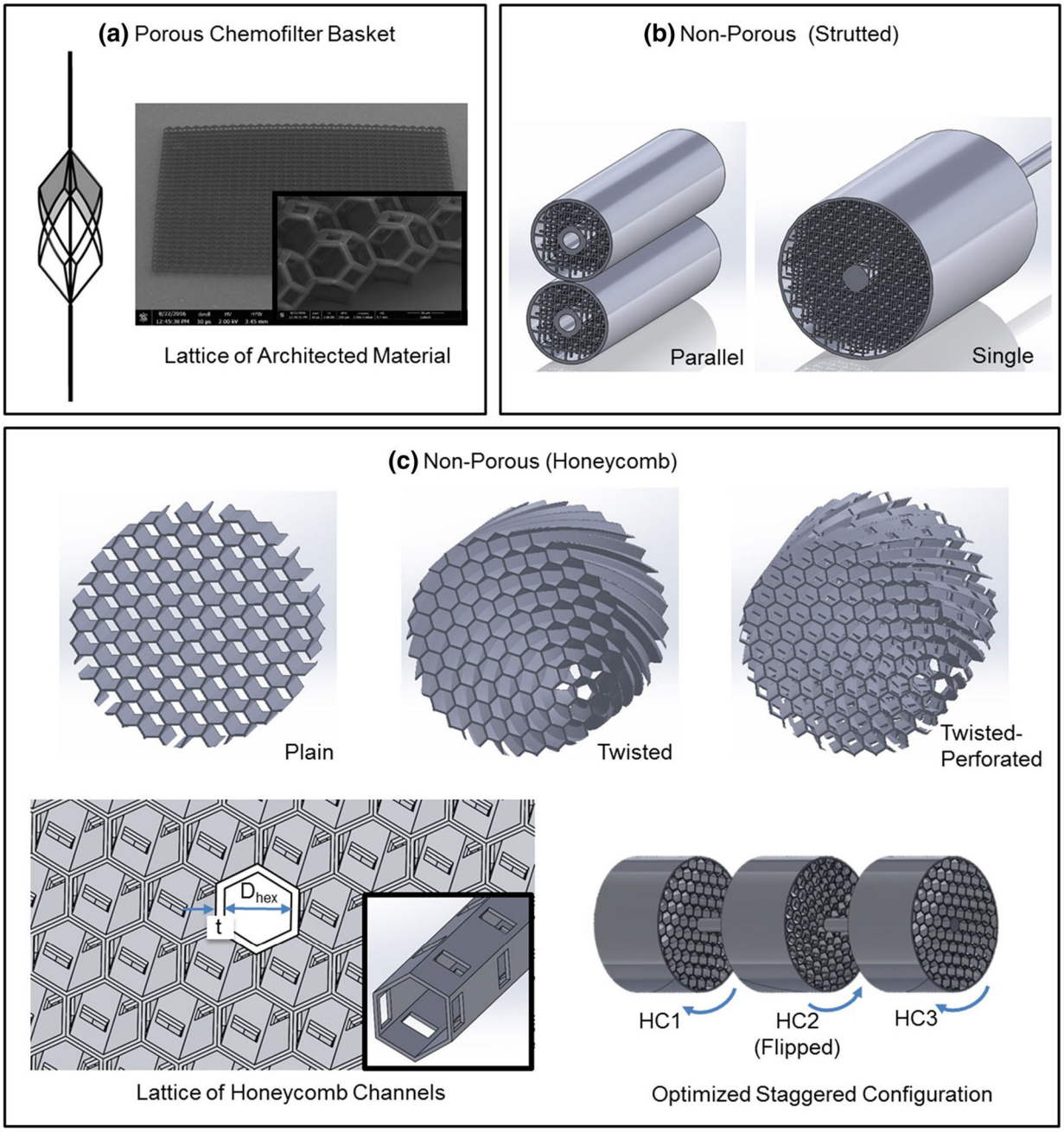

Fig. 2.

Chemofilter device configurations include **a** the porous Chemofilter basket (considered previously in Maani et al. 2018), **b** the non-porous strutted Chemofilter (tested experimentally by Oh et al. 2019), and **c** the non-porous honeycomb Chemofilter (developed in this study)

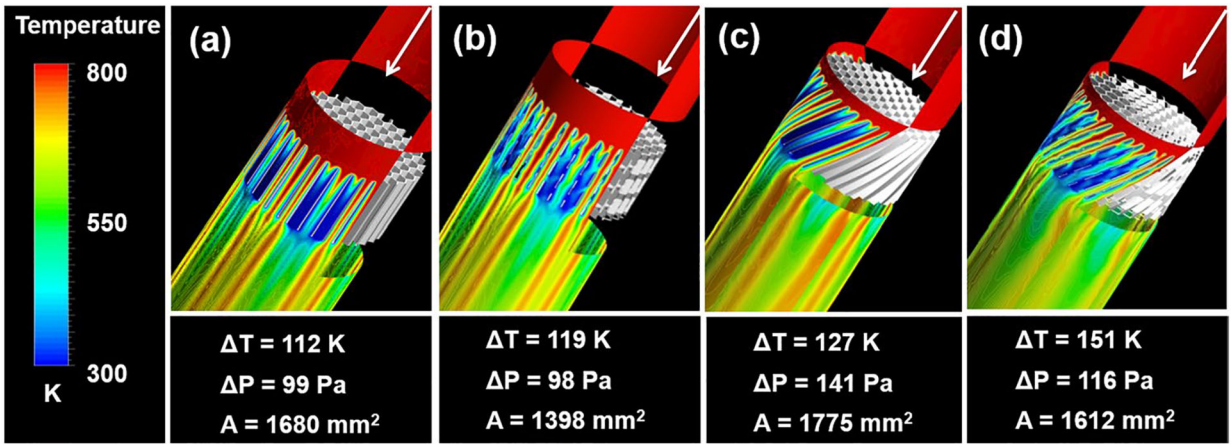

Fig. 3.

Thermal performance of different honeycomb Chemofilter configurations, each with parameters of L_{filter} = 5.8 mm, θ_{twist} = 45°, D_{hex} = 0.90 mm. Configurations include: **a** Plain, **b** Perforated, **c** Twisted, **d** twisted & perforated channels

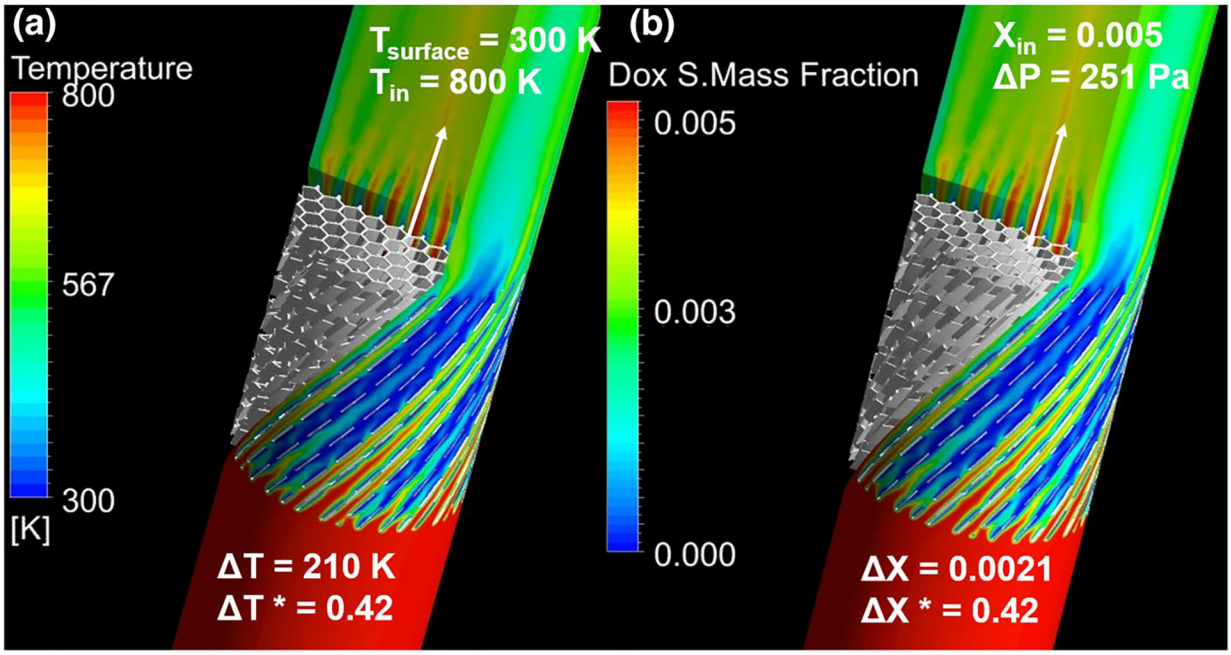

Fig. 4.

Comparison of heat and mass transport results for honeycomb Chemofilter with configuration parameters of L_{filter} = 10 mm, θ_{twist} = 45°, D_{hex} = 0.90 mm

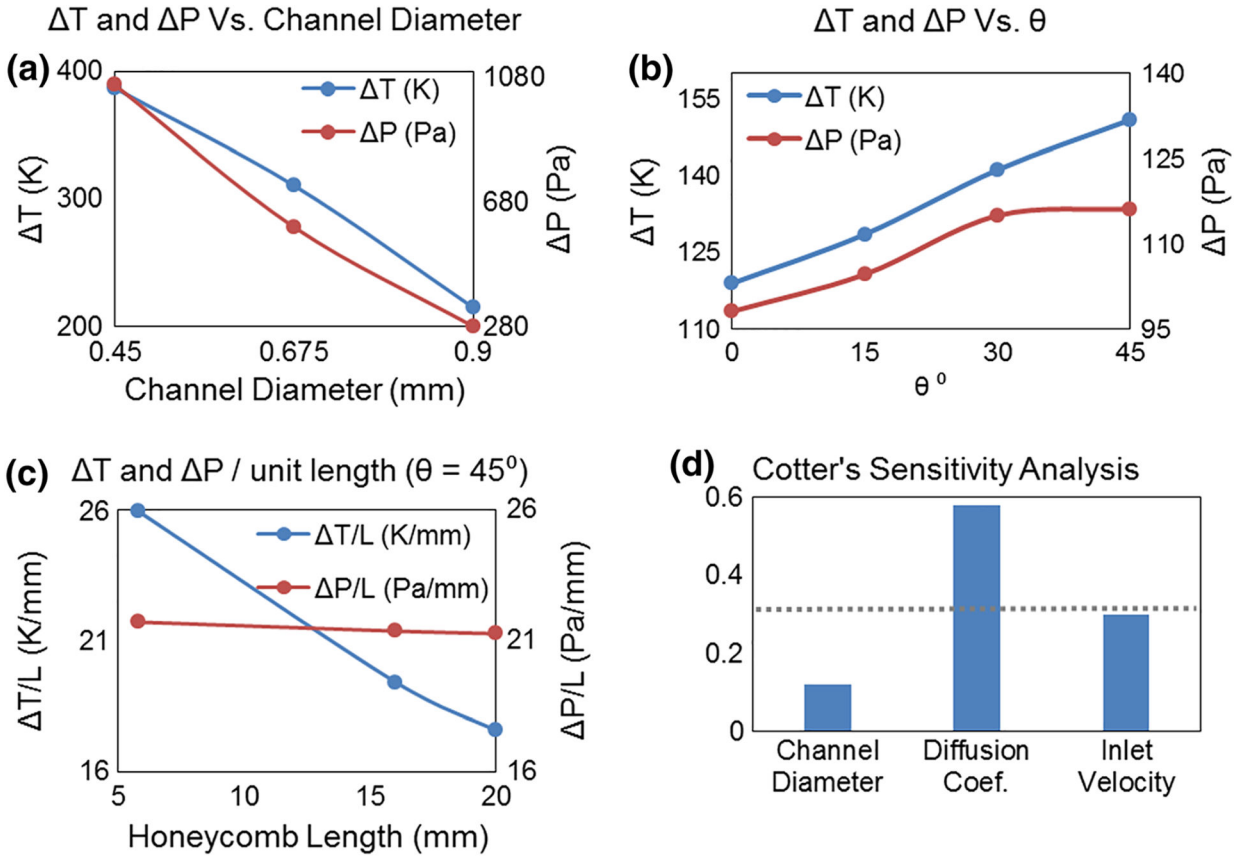

Fig. 5.

Evaluation of temperature and pressure drop as a function of **a** channel diameter, D_{hex} (θ_{twist} = 0, L_{filter} = 16 mm), **b** twist angle, θ_{twist} (L_{filter} = 5.8 mm, D_{hex} = 0.90 mm), and **c** unit filter length, L_{filter} (θ_{twist} = 45, D_{hex} = 0.90 mm). All data points were generated using diffusion coefficient α = 1e-7 m^2/s. **d** Cotter's sensitivity analysis investigating D_{hex}, velocity, and diffusion coefficient

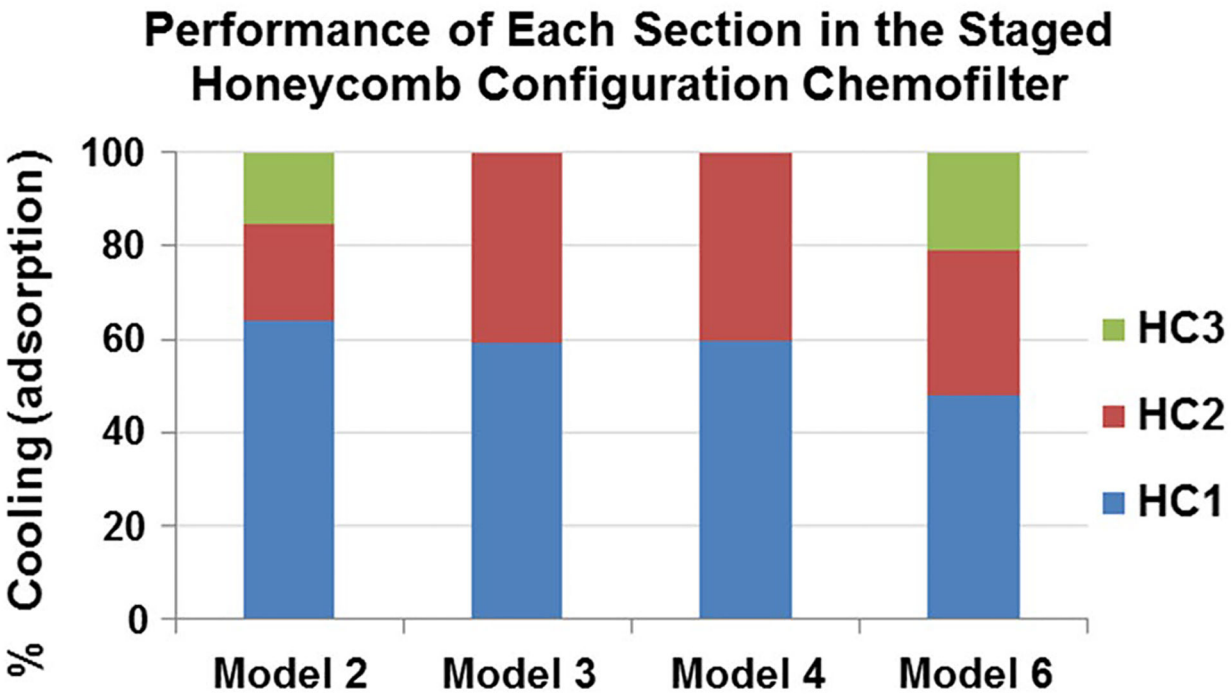

Fig. 6.

Percentage of cooling in each section of the staged honeycomb configuration models. (Model #'s from Table 2)

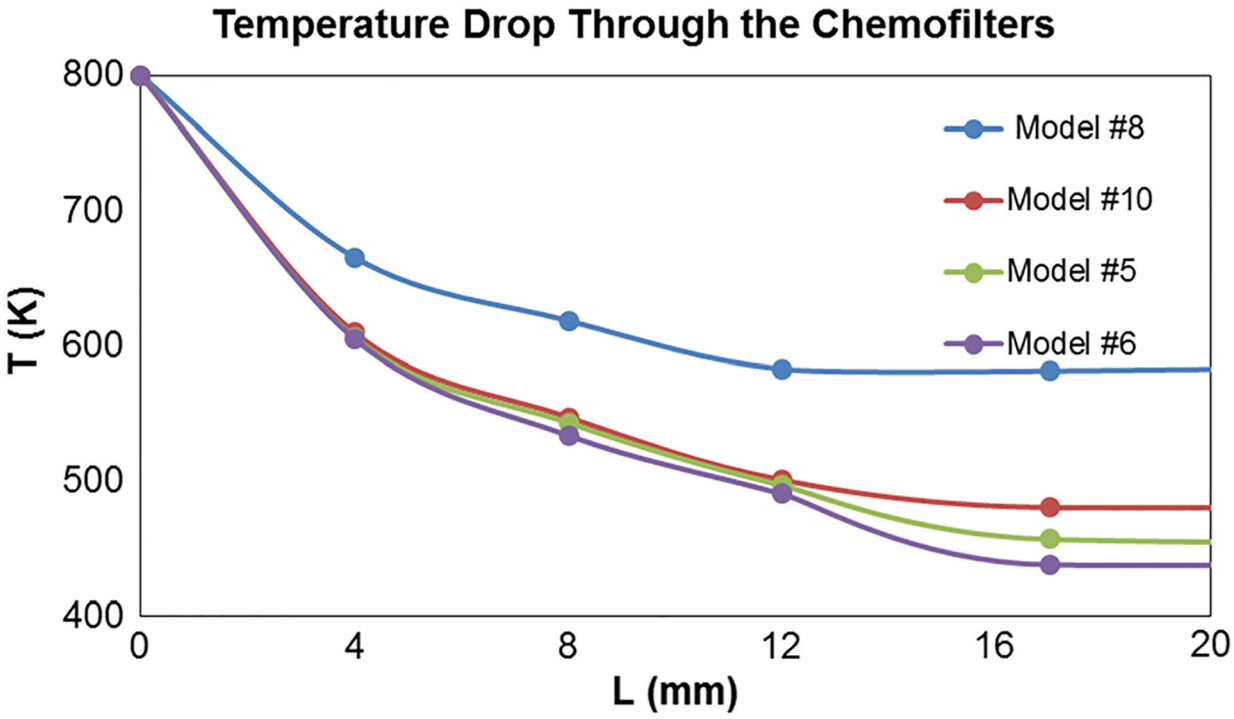

Fig. 7.
The temperature drop along the length of different Chemofilter configurations

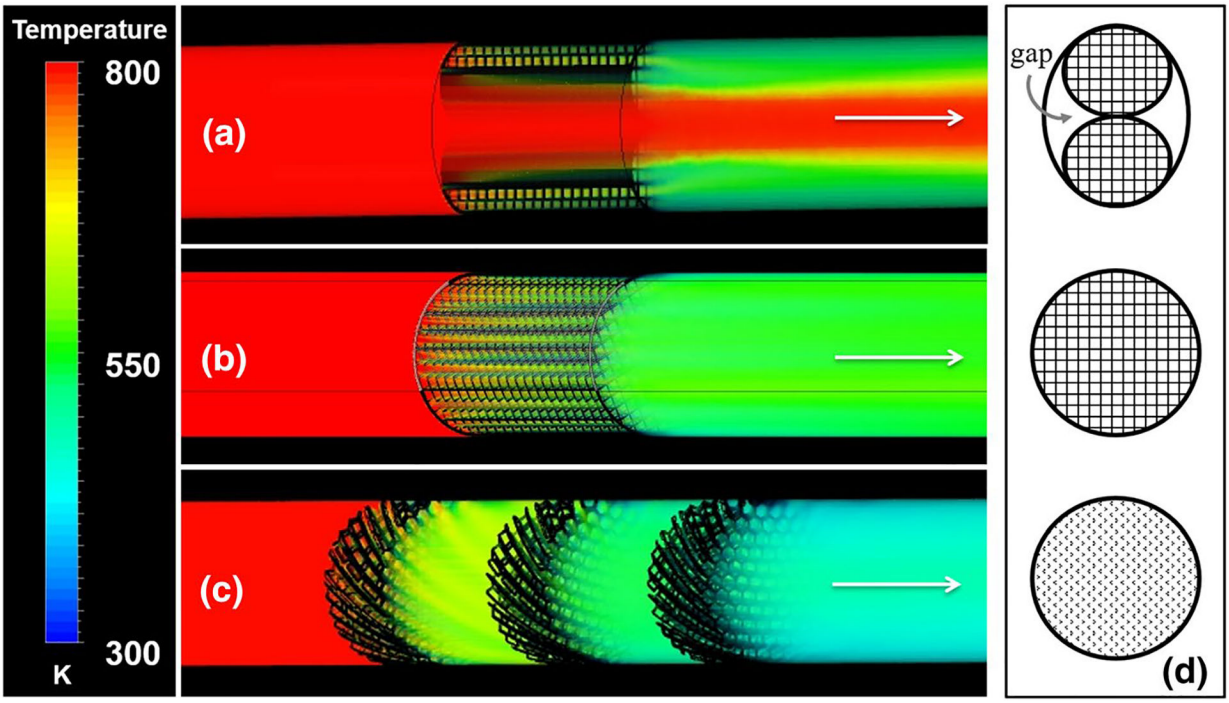

Fig. 8.

The temperature drop through **a** parallel strutted, **b** single strutted, and **c** staged honeycomb configurations. **d** A cross-sectional view through each configuration, **a**–**c**

Table 1

Summary of parameters with respective ranges varied during optimization of the Honeycomb configuration Chemofilter

Parameter	D_{Hex}[a] (mm)	Velocity[a] (m/s)	θ_{twist} (°)	L_{Filter} (mm)	Spacing (mm)	D[a] (m^2/s)
Range	0.45–0.90	0.01–0.10	0–45	5.8–30	1.3–11.6	10^{-9}–10^{-10}

D_{Hex}, the hexagonal channel diameter; θ_{twist}, the twist angle; L_{Filter}, the length of the Chemofilter; Spacing, the distance between the stages of honeycomb; D, the diffusion coefficient

[a]Denotes parameters considered for the Cotter's sensitivity analysis

Table 2

Comparison of six representative continuous and staged honeycomb configuration models

Model #	θ_{twist}	Configuration	L_{filter} (mm)	$A_{surface}$ (mm^2)	ΔT (K)	ΔP (Pa)	$\Delta T/L$ (K/mm)	$\Delta P/L$ (Pa/mm)
1	30°	Continuous	20	5420	319	371	16.0	18.6
2		Staged (3 sections) 1.3 mm spacing	5.8 × 3	4710	304	337	17.5	19.4
3		Staged (2 sections) 5.8 mm spacing *Flipped*	5.8 × 2	3140	243	240	20.9	20.7
4		Staged (2 sections) 5.8 mm spacing	5.8 × 2	3140	237	227	20.5	19.5
5	45°	Continuous	20	5570	352	425	17.6	21.3
6		staged (3 sections) 11.6 mm spacing	5.8 × 3	4840	334	391	19.2	22.5

Table 3

Comparison of strutted and continuous honeycomb configurations

Model (#)	Configuration (16 mm length)		Area (mm^2)	ΔT (K)	ΔP (Pa)	$\Delta T/L$ (K/mm)	$\Delta P/L$ (Pa/mm)	Temperature drop (%)
7	Strutted	Parallel	2050	117	146	7.30	9.10	23.4
8		Single	1950	202	288	12.6	18.0	40.4
9	Honeycomb	Plain	4590	215	281	13.4	17.6	43.0
10		Twisted-perforated	4460	311	342	19.4	21.4	62.2